Supplementary Information

Rich oxygen vacancies, mesoporous TiO$_2$ derived from MIL-125 for high-efficient photocatalytic hydrogen evolution

Tianping Lv,[§] Bin Xiao,[§] Shiqiang Zhou, Jianhong Zhao, Tai Wu, Jin Zhang, Yumin Zhang,* Qingju Liu*

Yunnan Key Laboratory for Micro/Nano Materials & Technology, National Center for International Research on Photoelectric and Energy Materials, School of Materials and Energy, Yunnan University, Kunming 650091, P. R. China.

 [§] These authors contributed equally to this work

*Corresponding author: Yumin Zhang, E-mail:zhangyumin@ynu.edu.cn, Tel: +138 0872 5319; Qingju Liu, E-mail: qjliu@ynu.edu.cn. Tel: +86 0871 65032713.

Experimental section

Chemicals. Tetrabutyl titanate (TBOT), 1, 4-benzenedicarboxylic acid and N, N-Dimethylformamide (DMF) were purchased from Aladdin Chemical Reagent Co., Ltd. (China). The methanol was purchased from General-Reagent Co., Ltd. Commercial P25 was purchased from Beijing Chemical Co., Ltd. Deionized water was obtained at room temperature and the resistance of 18.25 MΩ. All commercially available reagents and solvents were used as received without further purification.

Preparation of mesoporous TiO$_2$ with rich oxygen vacancies. The metal organic framework precursor MIL-125 was obtained according to the typical synthesis previously reported procedure.[1] The specific steps are as follows, dissolved 3 g 1, 4-benzenedicarboxylic acid in 54 ml DMF, added 6 ml methanol and 1.56 ml TBOT mixed solution into the above solution under magnetic stirring, until the mixed solution became a transparent and clear liquid. The solution was placed in an oil bath at 130℃ to react for 24 h. After cooling to room temperature, a white precipitate was obtained by centrifugation, and then washed with DMF and methanol three times, respectively. Finally, the free solvent was removed overnight by vacuum drying at 60℃. The synthesized MIL-125 was sintered in the air at 350℃, 400℃, 450℃ and 500℃ with a heating rate of 10 ℃/min for 4 h, respectively, to obtain a cake-like mesoporous TiO$_2$ rich oxygen vacancies, which was denoted as MPT350, MPT400, MPT450 and MPT500.

Characterization. X-Ray diffraction (XRD) patterns, obtained on an X-ray diffractometer (Rigaku, Japan) using Cu-K$_\alpha$ irradiation (λ=1.5418 A), were used to determine the phase structures of the obtained samples. The accelerating voltage and applied current were 40 kV and 80 mA, respectively. The morphology and microstructure of the samples were examined by emission scanning electron microscope (FE-SEM, Nova nanoSEM 450, USA) and transmission electron microscope (TEM, JEM-2100, Japan). The Brunauer–Emmett–Teller (BET) specific surface area of the powders was analyzed by 3H-2000PS2 sorption analyzer, and the porosity of the samples was evaluated on the basis of nitrogen adsorption isotherms, measured at 77 K. Thermogravimetric-differential thermal analysis (TG-DTA) was

performed at a heating rate of 10°C/min (ZRT-B). The UV-vis diffuse reflection spectra (DRS) were recorded by a UV-vis spectrometer (Japan, Hitachi, U4100, referenced by $BaSO_4$) equipped with an integrating sphere accessory in the diffuse reflectance mode. X-ray photoelectron spectroscopy (XPS) measurements were accomplished via a photoelectron spectrometer (Thermo ESCALAB 250Xi, USA) with an Al Kα radiation source ($h\nu$ = 1486.6 eV). Photoluminescence (PL) spectra were obtained by a FL4500 fluorescence spectrophotometer (Shimadzu). The excitation wavelength was 320 nm, the scanning speed was 1200 nm min^{-1}, and the PMT voltage was 700 V. The widths of the excitation slit and emission slit were both 5.0 nm. The electron spin resonance (EPR) spectroscopy was performed on Bruker EMX to detect the unpaired electrons of TiO_2 powder at room temperature.

Photocatalytic measurements. The photocatalytic hydrogen evolution experiments were performed on the full glass automatic on-line trace gas analysis system (Fig. S14a, Labsolar-6A, Perfect Light Co. Ltd. Beijing). With Labsolar-6A, a 300W Xe lamp (Perfect light PLS-SXE300C; light intensity: 200 mW/cm^2) was used as the simulated sunlight source. The as-prepared catalyst (10 mg) was uniformly dispersed by using a magnetic stirrer in 120 mL of aqueous solution (containing H_2O/methanol, v/v=90:30). The temperature of the reaction was kept at 283 K by cool flowing water. Prior to photocatalytic water splitting reaction, the sealed system was completely degassed to remove dissolved air in the aqueous solution by purging with high-purity Ar gas for 0.5 h. During the irradiation process, a hydrogen sample (0.4 mL) was extracted from the reactor at a given interval and the amount of hydrogen produced was analyzed by an online gas chromatograph (GC7900). For the recycling experiment, the photocatalyst powder was dispersed into 120 mL of methanol solution (25vol.%), then the sealed system was purged with high-purity Ar gas to remove the dissolved air in the solution. During the continuous irradiation of 5 h in each cycle, a gaseous sample (0.4 mL) was extracted from the reactor at a given interval of 1 h to analyze the H_2 yield by using gas chromatograph with a thermal conductivity detector. After finishing one cycle, the sealed system needed to be degassed for removing the generated H_2. Meanwhile, the cooling water was used to maintain the temperature at 283 K. The determination of the

apparent quantum efficiency (AQE) for H_2 generation was performed using a Multichannel photochemical reactor (PCX50C Discover, Perfect Light Co. Ltd. Beijing) under the 365 nm LED light source as shown in Fig. S14b. The quantum efficiency is calculated by the following equation:

$$AQE = \frac{2MN_A hc}{AIt\lambda} \times 100\%$$

where M is the amount of hydrogen molecules, N_A is the Avogadro's constant, h is the Planck constant, c is the light velocity, I is the intensity of the light, A is the irradiation area, t is the reaction time, and λ is the wavelength of light.[2]

Photoelectrochemical measurements. The electrodes were prepared on fluorine-doped tin oxide (FTO) glass slides, which were cleaned with ethanol, rinsed with DI water, and dried prior to use. A total of 10 mg of the prepared samples were added into 200 μL of ethanol and 800 μL water with 10 μL of Nafion (5wt.%) and then carefully ground for a little while to form a homogenous slurry. Subsequently, the obtained slurry was evenly distributed onto the conductive side of FTO glass by the doctor blading technique. The effective area of the present electrodes is ca. 0.5 cm². After drying in the air, the photoelectron chemical properties of the obtained electrodes were tested in a three-electrode system on a Shanghai Chenhua CHI-760E electrochemical workstation. The prepared electrode, Pt wire, and Ag/AgCl electrode were used as the working, counter, and reference electrodes, respectively. The electrolyte was 0.2 M Na_2SO_4 aqueous solution, and the light source was a 300 W xenon lamp to provide visible light illumination. The Mott–Schottky plots were recorded by employing the impedance–potential mode in the scan voltage range of -1 V to 1 V at 500 Hz with an AC voltage amplitude of 10 mV. The photocurrent responses based on the amperometric I–t curves were obtained by measuring the change of photocurrent with time under repeatedly interrupted visible light irradiation. Electrochemical impedance spectroscopy (EIS) measurements were detected at a voltage of 5 mV applied to the electrodes with the frequency range of 10^5 to 0.1 Hz.
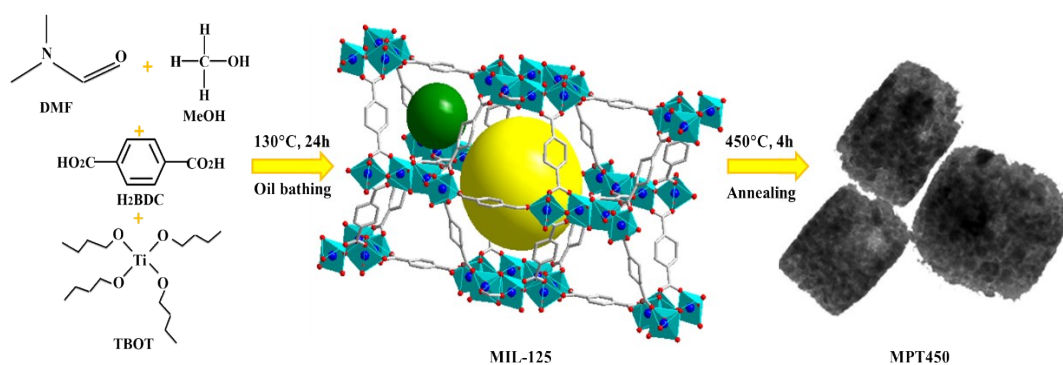
Fig. S1 Schematic illustration of the preparation of MPT450 photocatalyst.

The MPT450 photocatalyst were fabricated by high temperature annealing of MIL-125, which mainly involves two steps. Firstly, MIL-125 was prepared, its basic composition is $Ti_8O_8(OH)_4-(O_2C-C_6H_5-CO_2)_6$, which is composed of cyclic octamers constructed from sharing corner or edge of titanium oxide octahedron. These octamers are connected to the other 12 cyclic octamers via BDC linkers to form a porous three-dimensional quasi-cube structure, which contains two types of cages, an octahedron (12.5Å) and a tetrahedron (6Å).[3]
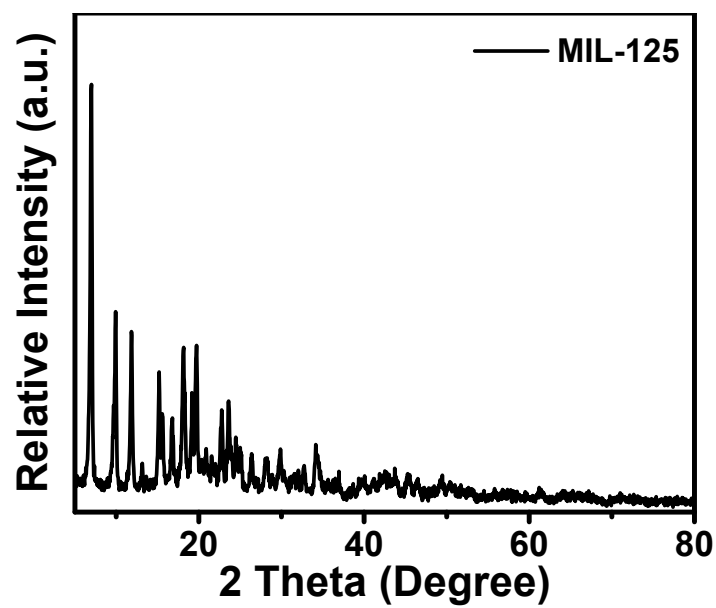
Fig. S2 XRD pattern of MIL-125.

The characteristic peaks of MIL-125 are in good agreement with the report of Meenakshi group,[4] indicating the successful preparation of MIL-125.
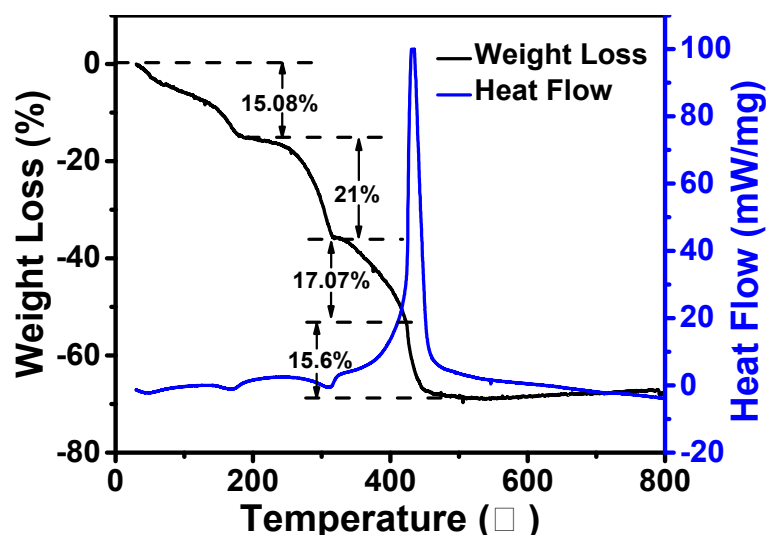
Fig. S3 TG/DTA pattern of MIL-125.

TG/DTA curves of MIL-125 shows the weight loss when heated from room temperature to 800℃. It can be obtained from the TG curve that there is a weight loss close to 15.08% from room temperature to 200°C, indicating that some volatile substances adsorbed in the MIL-125 pores desorbed with the increase of temperature. As the temperature continued to rise to 350°C, MIL-125 had a severe weight loss (about 21%), which was caused by the release of organic matter in the frame at high temperature. The third weight loss (about 17.07%) between 350~400°C corresponds to the degradation of the MIL-125 framework structure to generate anatase phase TiO_2. At 400~450°C, the weight loss (about 15.6%) continues, and there is an exothermic peak on the DTA curve, which was caused by the transition of TiO_2 from anatase phase to rutile phase. After heating to 450°C, the weight of the sample basically remains constant.
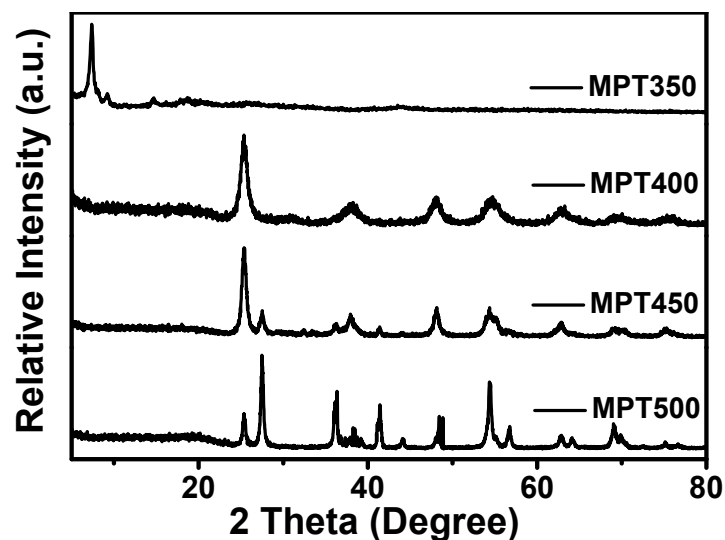
Fig. S4 XRD patterns of MIL-125 under different sintering temperature for 4 hours.

The XRD pattern of MIL-125 annealing at different temperatures can also prove its changing process. At the annealing of 350℃, the framework structure of MIL-125 began to degrade, but the characteristic peak of TiO_2 has not yet appeared. At 400℃, the characteristic peak of anatase phase TiO_2 appeared. When the annealing temperature reached 450℃, the crystallization peak strengthened and the rutile phase appeared in the sample, indicating that TiO_2 underwent phase transition between 400~450℃. With the annealing to 500°C, TiO_2 is dominated by rutile phase, so 450°C is selected as the annealing temperature of MIL-125.
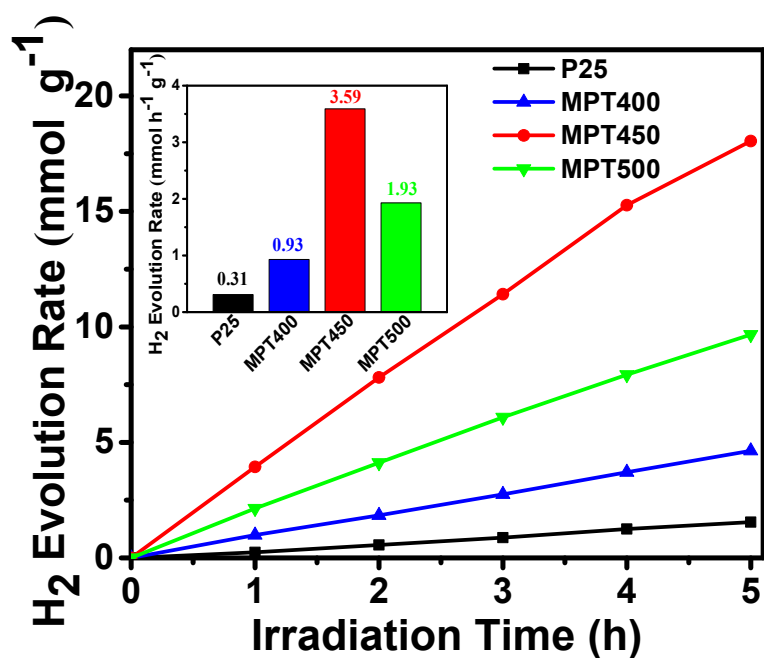
Fig. S5 Photocatalytic activity of MIL-125 sintered samples at different annealing temperatures under 300W Xe lamp (light intensity: 200 mW/cm^2), inset shows the hydrogen evolution rate.

The photocatalytic hydrogen evolution performance of the samples at different annealing temperatures was tested. The MPT350 remained the patterns of MIL-125, not form TiO$_2$ (Fig. S4), so the hydrogen evolution performance was not compared. It can be seen that the photocatalytic hydrogen evolution increases with the increase of sintering temperature. At 450℃ (MPT450), the hydrogen evolution rate of the catalyst reaches the maximum value of 3.59 mmol g^{-1} h^{-1}.
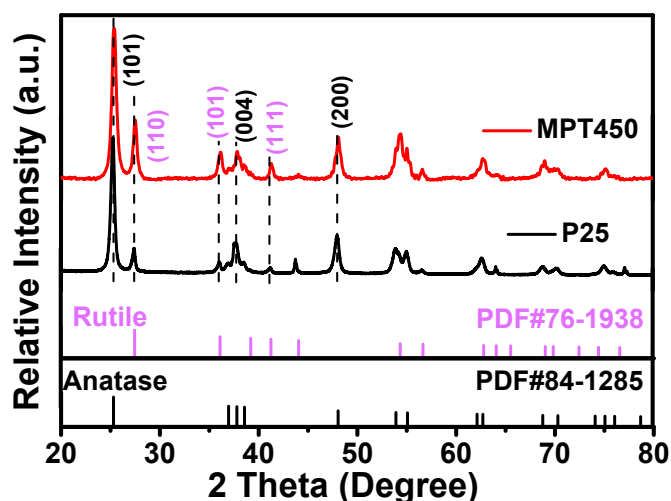
Fig. S6 XRD patterns of P25 and MPT450.

The crystal structures of MPT450 and reference sample (P25) were investigated by XRD. As shown in Fig. S6, P25 consists of anatase phase (PDF#84-1285) and rutile phase (PDF#76-1938). Well-defined diffraction angles (2θ) at 25.365, 37.799, 48.038º and 27.440, 36.078, 41.239º can be indexed as the (101), (004), (200) planes of anatase phase TiO_2 and the (110), (101), (111) planes of rutile phase TiO_2, respectively. Table S1 shows the content of anatase and rutile phase in MPT450 and P25 samples. The C peak was searched on the XRD pattern of MPT450, and no corresponding peak was found to match the C spectrum. Compared with the abovementioned data, the anatase and rutile phases of MPT450 reveals diffraction angles at 25.321, 37.862, 48.062º and 27.492, 36.149, 41.321º, respectively, which is shifted toward higher angle, indicating that the crystal interplanar distance of MPT450 decreased. The change of crystalline structure may be caused by low-coordinated surface atoms or the existence of surface defects in TiO_2, such as oxygen vacancies (V_O).[5]
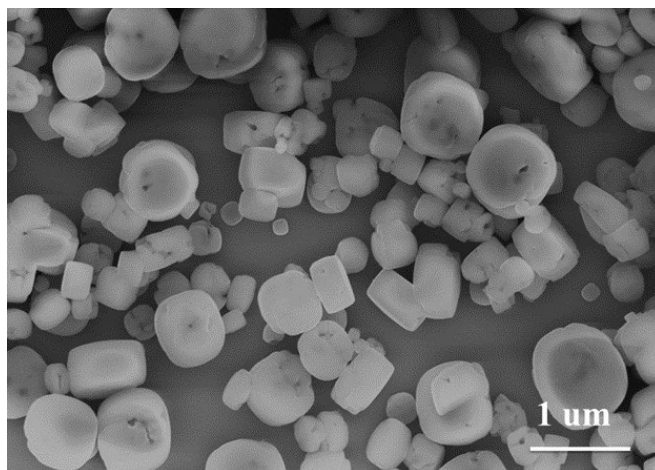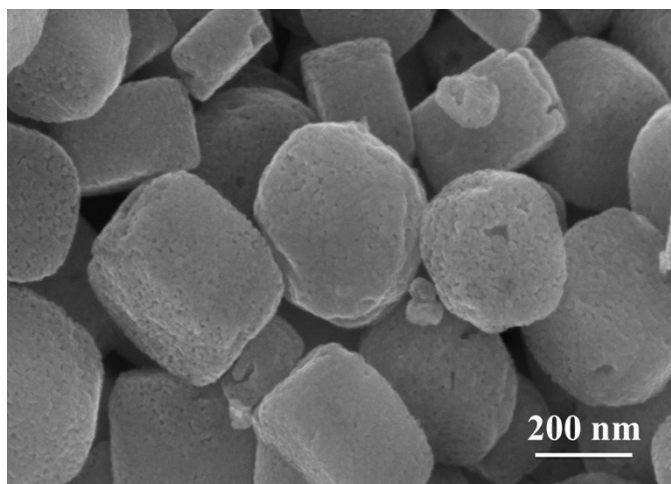
Fig. S7 SEM images of MIL-125.
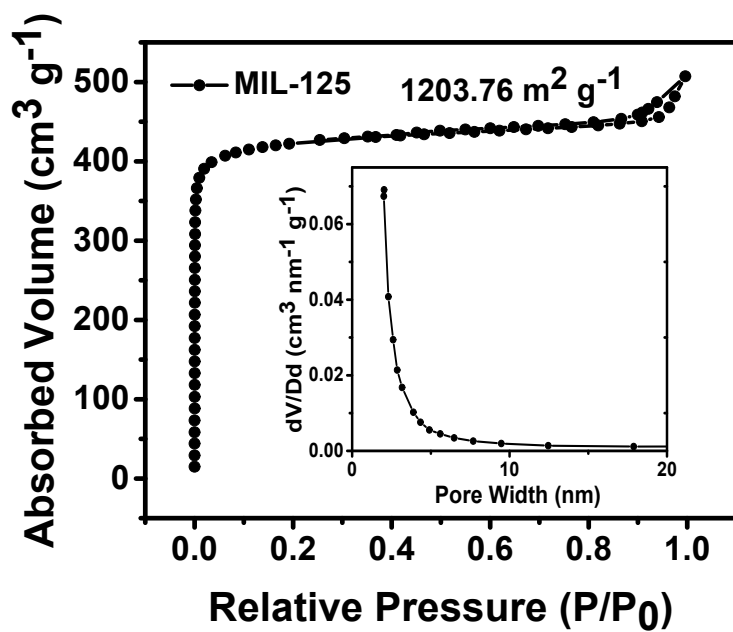
Fig. S8 SEM images of MPT450.

Fig. S9 N$_2$ adsorption-desorption isotherm of MIL-125. Inset: the corresponding pore size distribution plot calculated by the Barrett-Joyner-Halenda (BJH) method from the adsorption branch.
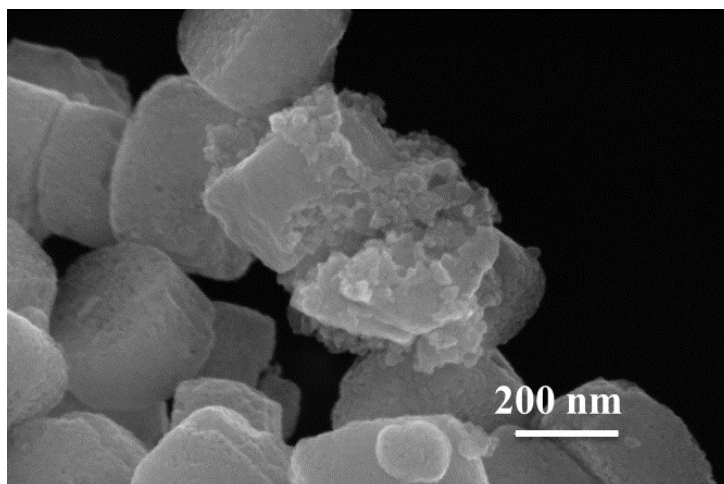
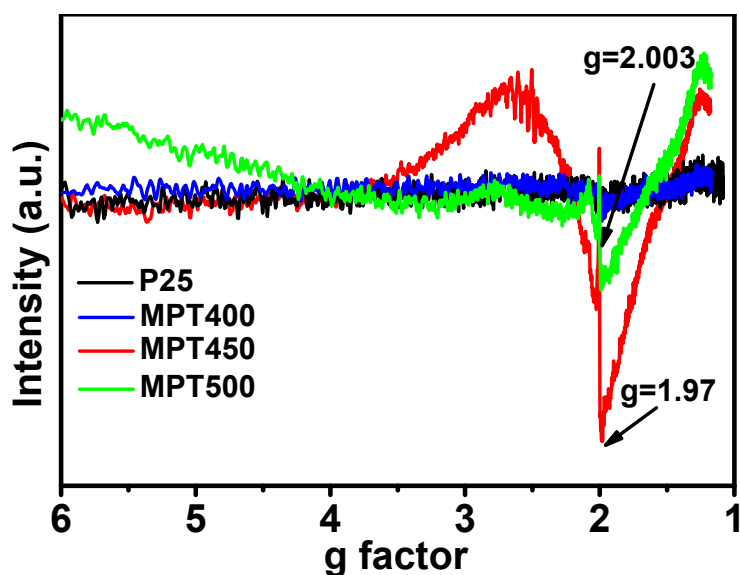Fig. S10 SEM image of fragmentized MPT450.

Fig. S11 EPR spectra of MIL-125 sintered samples at different annealing temperatures and P25 under room temperature.

In the process of MIL-125 forming TiO_2 by annealing, Ti in MIL-125 reacts with the nearby with the nearby oxygen and aggregates into stable TiO_2 nanoparticles.[6] Meanwhile, the high-temperature decomposition of organic ligands requires a large amount of oxygen, which is easy to extract oxygen from TiO_2, release active oxygen and electrons, and forms oxygen vacancy.[7] When the annealing temperature is lower than 450℃, the organic ligand cannot be wholly removed, thus there are not that much oxygen vacancies can be formed. While, if the annealing is higher than 450℃, not only the organic ligands are removed, but also the defects can be compensated. Thus the amount of oxygen vacancy reach the highest at the annealing temperature of 450℃. The oxygen vacancies analysis of samples with different annealing temperatures was carried out by EPR, as shown in Fig S11. It can be seen that MPT450 shows the strongest single of oxygen vacancy, indicating MPT450 possesses the most amount of oxygen vacancies. This was consistent with the above analysis results and the efficiency of photocatalytic hydrogen evolution (Fig. S5).
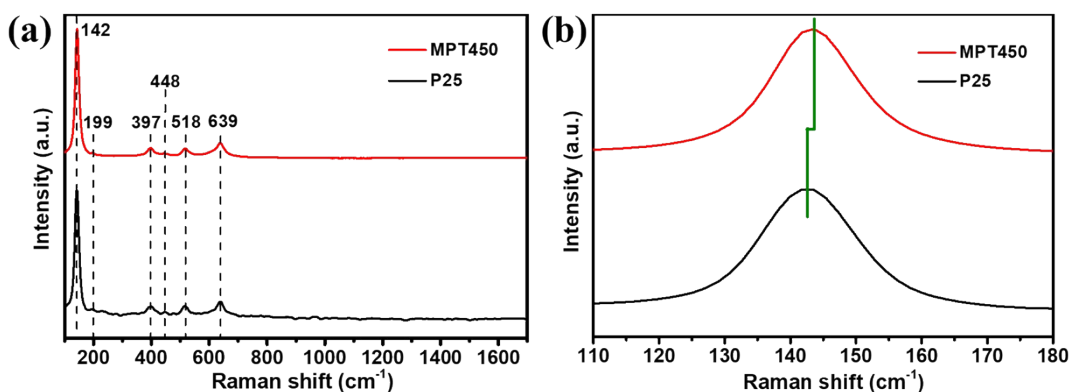
Fig. S12 Raman spectra of P25 and MPT450.

Structural properties of MPT450 and P25 were further examined by measuring Raman scattering spectra. Raman peaks at near 142cm⁻¹, 199cm⁻¹, 397cm⁻¹, 518cm⁻¹, 639cm⁻¹ and 448cm⁻¹ correspond to the anatase and rutile crystal structures of TiO_2, respectively (Fig. S12a) [8]. Importantly, local magnified Raman spectra show a shift of peak value toward higher wavenumber in MPT450 compared to P25 as displayed in Fig. S12b. This phenomenon can be attributed to phonon confinement as a result of the presence of oxygen vacancies in MPT450 [9].
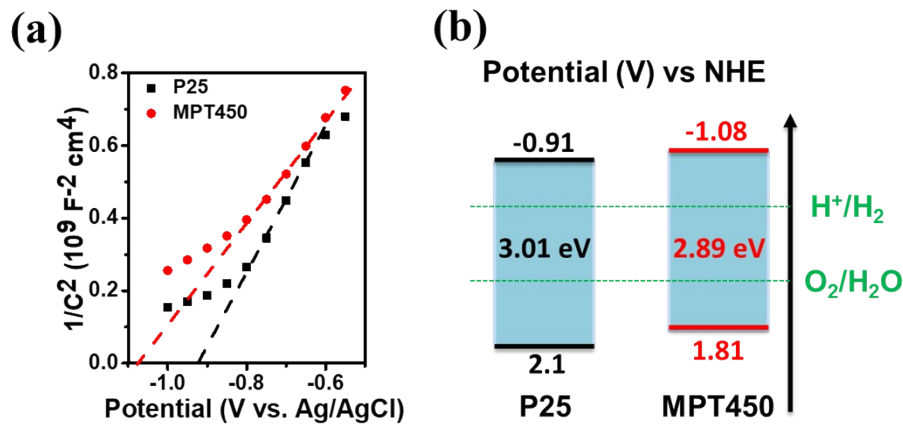
Fig. S13 (a) The Mott-Schottky plots and (b) the energy band structure of MPT450 and P25.

Under dark conditions, the capacitance measurement was tested at a frequency of 0.5 kHz to determine carrier density (N_d) of MPT450 and P25 based electrodes according to the following formula:

$$N_d = (2/e_0\varepsilon\varepsilon_0)[d(1/C^2)/dV]^{-1} \qquad (1)$$

where N_d is the electron carrier density, e_0 is the elemental charge, ε is relative permittivity of the semiconductor, ε_0 is the permittivity of vacuum, $d(1/C^2)/dV$ is the straight slop.[10] From Fig. S13a, the flat band potentials in the Mott-Schottky plots of P25 and MPT450 are approximately -0.91 V and -1.08 V, respectively, relative to the Ag/AgCl electrode. In general, the conduction band potential (E_{cb}) of an n-type semiconductor is more negative -0.1 V or -0.2 V than the flat band potential.[11] Therefore, relative to the Ag/AgCl electrode, the conduction band potential of P25 and MPT450 can reach approximately -1.11 V and -1.28 V, which is compared with the normal hydrogen electrode (NHE) ($E_{NHE} = E_{Ag/AgCl}+0.197$ V), the conduction band potentials are -0.91 V and -1.08 V, respectively.[12] According to the calculation formula $E_{vb} = E_{cb} + E_g$ at the standard hydrogen electrode, the valence band potentials of P25 and MPT450 are 2.1 V and 1.81 V, respectively.[13] The valence band and conduction band potentials of P25 and MPT450 are shown in Fig. S13b and Table S4.
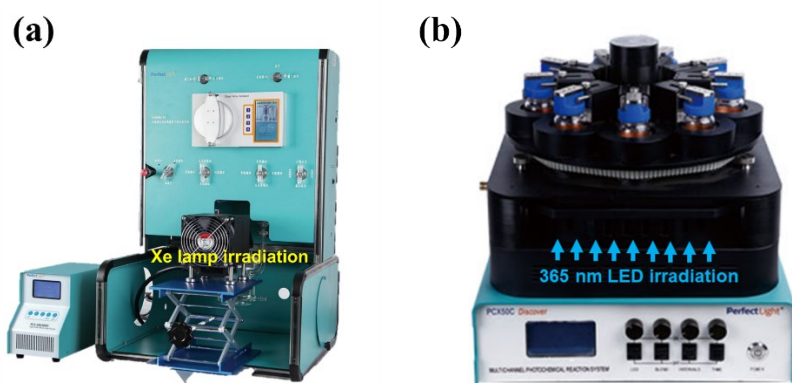
Fig. S14 (a) Full glass automatic on-line trace gas analysis system with Xe lamp (Labsolar-6A, Perfect Light Co. Ltd. Beijing), (b) Quantum yield measurement system (PLD-QY1000, Perfect Light Co. Ltd. Beijing).

Table S1 Anatase and rutile content of P25 and MPT40, samples.

Samples	P25	MPT450
Anatase content (%)	88.92	78.33
Rutile content (%)	11.08	21.67

Table S2 The S_{BET}, pore volume and average pore width of MIL-125, P25 and MPT450.

Samples	S_{BET} ($m^2 g^{-1}$)	Pore volume ($cm^3 g^{-1}$)	Average Pore width (nm)
MIL-125	1203.76	0.75	2.51
P25	52.8	0.22	17.20
MPT450	176.9	0.14	3.18

Table S3 A brief survey of the photocatalytic hydrogen production performance of TiO$_2$

photocatalysts reported in literature.

Photocatalyst	HER rate (umol g^{-1} h^{-1})	Light sourse	Cocatalyst	Reaction condition	Ref.
MPT450	3590	Xe lamp (300W)		Methanol aqueous solution (25 vol%)	This work
TiO$_2$(B)	690	Xe lamp (350W)		Methanol aqueous solution (20 vol%)	14
TiO$_2$/Graphene-700	2894	Xe lamp (300W)		Methanol aqueous solution (20 vol%)	15
Triphasic TiO$_2$	3570	Xe lamp (300W)	1.0wt% Au	Methanol aqueous solution (25 vol%)	16
TiO$_2$(B)/RP	380	Xe lamp (300W)	3.0wt% Pt	Pure water	17
TiO$_2$	1221	Xe lamp (1000W)		Ethanol aqueous solution (4.28 mol/L)	18
FeS$_2$-TiO$_2$	100	Xe lamp (300W)		Methanol aqueous solution (50 vol%)	19
TiO$_2$ NBs	1363	Xe lamp (300W)	1.0wt% Pt	Methanol aqueous solution (10 vol%)	20
TiO$_2$/Ti$_2$O$_3$	1440	Xe lamp (300W)		Methanol aqueous solution (20 vol%)	21
Co-TiO$_2$	1682	Xe lamp (300W)		Methanol aqueous solution (20 vol%)	22
Bi$_2$O$_2$Se/TiO$_2$	1240	Xe lamp (300W)		Glycerol aqueous solution (5 vol%)	23
TiO$_2$@MOF FS	440	Xe lamp (300W)		Triethanolamine aqueous solution (8 vol%)	24

Table S4 Calculated E$_{CB}$ and E$_{VB}$ for P25 and MPT450.

Semiconductor	E_g/eV	E_{cb}/eV	E_{vb}/eV
P25	3.01	-0.91	2.1
MPT450	2.89	-1.08	1.81

References

1   X. B. Zhao, J. H. Zhao, J. C. He, B. Li, Y. M. Zhang, J. C. Hu, H. P .Wang, D. M. Zhang and Q. J. Liu, *ACS Appl. Energy Mater.*, 2020, **3**, 6180-6187.

2   W. Zhang, H. L. He, Y. Tian, H. Z. Li, K. Lan, L. H. Zu, Y. Xia, L. L. Duan, W. Li and D. Y. Zhao, *Nano Energy*, 2019, **66**, 104113.

3   S. N. Kim, J. Kim, H. Y. Kim, H. Y. Cho, W. S. Ahn, Catal. Today, 2013, 204, 85-93.

4   M. Dan-Hardi, C. Serre, T. Frot, L. Rozes, G. Maurin, C. Sanchez and G. Fe´rey, J. Am. Chem. Soc., 2009, 131, 10857-10859.

5   S. Hu, P. Z. Qiao, L. P. Zhang, B. J. Jiang, Y. T. Gao, F. Hou, B. G. Wu, Q. Li, Y. Jiang, C. G. Tian, W. Zhou, G. H. Tian and H. G. Fu, Appl. Catal., B, 2018, 239, 317-323.

6   Q. Qin, Y. Zhao, M. Schmallegger, T. Heil, J. Schmidt, R. Walczak, G. G. Demner, H. J. Jiao and M. Oschatz, *Angew. Chem. Int. Ed.*, 2019, **58**, 13101-13106.

7   X. L. Weng, Y. L. Zhang, F. Bi, F. Dong, Z. B. Wu and J. A. Darr, *J. Mater. Chem. A*, 2017, **5**, 23766-23775.

8   A. Naldoni, M. Allieta, S. Santangelo, M. Marelli, F. Fabbri, S. Cappelli, C. L. Bianchi, R. Psaro and V. D. Santo, *J. Am. Chem. Soc.*, 2012, **134**, 700-7603.

9   R. R. Jia, Y. T. Wang, C. H. Wang, Y. F. Ling, Y. F. Yu and B. Zhang, *ACS Catal.*, 2020, **10**, 3533-3540.

10   (a) T. W. Kim and K. S. Choi, *Science*, 2014, **343**, 990-994; (b) Z. B. Jiao, M. D. Shang, J. M. Liu, G. X. Lu, X. S. Wang and Y. P. Bi, *Nano Energy*, 2017, **31**, 96-104.

11   S. S. Yi, J. M. Yan, B. R. Wulan, S. J. Li, K. H. Liu and Q. Jiang, *Appl. Catal., B*, 2017, **200**, 477-483.

12   G. J. Ai, H. X. Li, S. P. Liu, R. Mo and J. X. Zhong, *Adv. Funct. Mater.*, 2015, **25**, 5706-5713.

13   L. J. Zhang, S. Li, B. K. Liu, D. J. Wang and T. F. Xie, *ACS Catal.*, 2014, **4**, 3724-3729.

14 J. J. Si, S. Y. Xiao, Y. Wang, L. B. Zhu, X. H. Xia, Z. B. Huang and Y. Gao, *Nanoscale*, 2018, **10**, 2596-2602.

15 J. P. Ji, Z. H. Li, C. C. Hu, Y. Sha, S. Y. Li, X. H. Gao, S. Y. Zhou, T. Qiu, C. Y. Liu, X. T. Su, Y. Hou, Z. Lin, S. D. Zhou, M. Ling and C. D. Liang, *ACS Appl. Mater. Interfaces*, 2020, **12**, 40204-40212.

16 H. L. Xiong, L. L. Wu, Y. Liu, T. N. Gao, K. Q. Li, Y. Long, R. Zhang, L. Zhang, Z. A. Qiao, Q. S. Huo, X. Ge, S. Y. Song and H. J. Zhang, *Adv. Energy Mater.*, 2019, **9**, 1901634.

17 Y. K. Zhu, J. Z. Li, C. L. Dong, J. Ren, Y. C. Huang, D. M. Zhao, R. S. Cai, D. X. Wei, X. F. Yang, C. X. Lv, W. Theis. Y. Y. Bu, W. Han, S. H. Shen and D. J. Yang, *Appl. Catal., B*, 2019, **255**, 117764.

18 Y. Alsalka, A. Hakki, J. Schneider and D. W. Bahemann, *Appl. Catal., B*, 2018, **238**, 422-433.

19 T. R. Kuo, H. J. Liao, Y. T. Chen, C. Y. Wei, C. C. Chang, Y. C. Chen, Y. H. Chang, J. C. Lin, Y. C. Lee, C. Y. Wen, S. S. Li, K. H. Lin and D. Y. Wang, *Green Chem.*, 2018, **20**, 1640-1647.

20 J. Liu, J. Ke, Y. Li, B. J. Liu, L. D. Wang, H. N. Xiao and S. B. Wang, *Appl. Catal., B*, 2018, **236**, 396-403.

21 J. Y. Chu, Y. C. Sun, X. J. Han, B. Zhang, Y. C. Du, B. Song and P. Xu, *ACS Appl. Mater. Interfaces*, 2019, **11**, 18475-18482.

22 X. Wu, S. W. Zuo, M. Qiu, Y. Li, Y. F. Zhang, P. F. An, J. Zhang, H. B. Zhang and J. Zhang, *Chem. Eng. J.*, 2020, **11**, 127681.

23 D. Ding, Z. Jiang, D. Ji, N. V. Myung and L. Zan, *Chem. Eng. J.*, 2020, **400**, 125931.

24 L. M. Sun, Y. S. Yuan, F. Wang, Y. L. Zhao, W. W. Zhan and X. G. Han, *Nano Energy*, 2020, **74**, 104909.